Journal of Materials Chemistry C

Accepted Manuscript

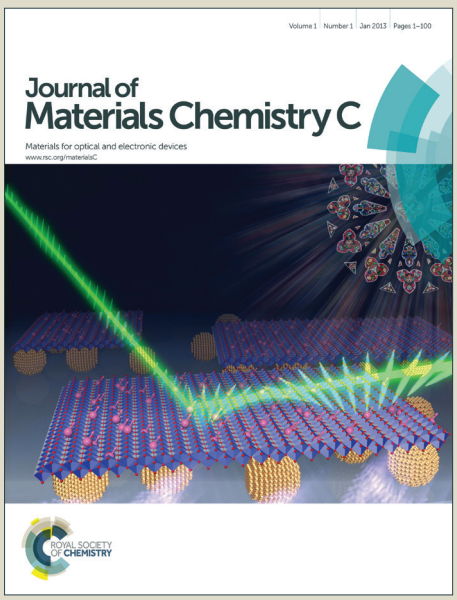

ROYAL SOCIETY OF CHEMISTRY

www.rsc.org/materialsC

Cite this: DOI: 10.1039/c0xx00000x

www.rsc.org/xxxxxx

ARTICLE TYPE

Blue to green emission and energy transfer between Ce^{3+} ions in $Ca_{15}Si_{20}O_{10}N_{30}$

Yanyan Li, Jianyan ding, Quansheng Wu, Qiang Long, Xicheng Wang and Yuhua Wang*

Received (in XXX, XXX) Xth XXXXXXXXX 20XX, Accepted Xth XXXXXXXXX 20XX

DOI: 10.1039/b000000x

A near-ultraviolet (near-UV) excited phosphor, $Ca_{15}Si_{20}O_{10}N_{30}:Ce^{3+}$, was synthesized by a solid state reaction, and the crystal structure and luminescence properties were investigated in detail. $Ca_{15}Si_{20}O_{10}N_{30}$ crystallizes in a cubic unit cell with space group $Pa\bar{3}$ and the lattice parameters were determined to be a = b = c = 15.4195 (3) Å. The maximum emission wavelength can be tuned from about 470 nm to 520 nm as the content of Ce^{3+} increases due to the energy transfer between various Ce^{3+} activators located at different coordination environments, which was verified by the time-resolved emission spectra (TRES) and the variation in decay rate with respect to the detection wavelength. Upon excitation at 365 nm, $Ca_{15}Si_{20}O_{10}N_{30}:Ce^{3+}$ exhibited a relatively low thermal quenching, and the T_{50} is measured to be 233 ℃. The above results indicate that $Ca_{15}Si_{20}O_{10}N_{30}:Ce^{3+}$ is a promising candidate for application in white light emitting diodes (white LEDs).

Introduction

There has been considerable interest in white light-emitting diodes (LEDs), which have become widely available as an environmentally friendly lighting system known as solid-state lighting (SSL), owing to their long operation lifetime, low energy consumption, high material stability, and so on.[1-3] Generally, two different configurations are possible for white LEDs, based on either a blue LED or a near-ultraviolet (UV) LED.[4, 5] The most widely used LEDs are combined blue LED chips with the yellow-emitting phosphor, but it has a deficient red emission, leading to its bluish-cold light owing to its high color temperature (CCT＞4500 K) and low color rendering index (CRI≈70-80). Thus, the development of new phosphors that can be effectively excited in the near-UV range would be a good impetus for the alternative approach to white LEDs.

To find novel efficient phosphors, the choice of the activator ions is one of the key factors. As a highly efficient activator with allowed 5d-4f transitions, the Ce^{3+} ion has been widely investigated because the emission and absorption spectra of Ce^{3+} ion usually consist of broad bands due to the transition between the $4f^1$ ground state and the crystal field components of the 5d excited state configurations.[6] Therefore, many Ce^{3+}-containing phosphors, including oxides, sulfides, have been proposed as color-converting materials for SSL. However, only a few Ce^{3+} doped oxide phosphors are genuine candidates for white LEDs since oxide hosts rarely offer excitation in the near-UV or blue part of the spectrum.[7] The garnet system, $(Y,Gd)_3(Al,Ga)_5O_{12}:Ce^{3+}$ (YAG:Ce^{3+}), is an important exception, exhibiting a large redshift in the 5d energy level of Ce^{3+} such that it absorbs in the blue and emits in the yellow.[8] It plays an important role in SSL based on blue LEDs. However, its excitation band matches with only blue light and restricts its application for near-UV LEDs.

During the past decade, Ce^{3+} doped (oxy)nitrides have attracted a great deal of attention as phosphors for use in LED applications.[9] The N^{3-} in these lattices is a soft Lewis base, which results in a high covalency. This shifts the energy of the 4f-5d absorption and emission for Ce^{3+} in these host lattices to sufficiently low energies. In addition, both the performance and stability of (oxy)nitrides have been proven to be superior to traditional oxide, halide and sulfide-based phosphors. Recently, a great number of (oxy)nitrides phosphors have been discovered, examples include β-SiAlONs,[10] $YSiO_2N$,[11] $Y_2Si_3O_3N_4$,[12] $MYSi_4N_7$ (M = Sr, Ba),[13, 14] $CaSiN_2$,[15] $LaSi_3N_5$,[16] $La_5Si_3O_{12}N$,[17] $La_4Si_2O_7N_2$,[17] $CaSi_2O_2N_2$,[18] and $Y_6Si_3O_9N_4$,[19] etc. However, only a small amount of them can be put into practical use. In this regard, the discovery of new Ce^{3+} doped (oxy)nitride phosphors with good luminescence properties has been a significant issue in the LED industry.[20]

K. S. Sohn[21] firstly discovered $Ca_{15}Si_{20}O_{10}N_{30}$ using the combi-chem method, and studied the Eu^{2+} luminescence from 5 different crystallographic sites in $Ca_{15}Si_{20}O_{10}N_{30}$, which is isostructural with $Ca_{15}Al_2Si_{18}O_{12}N_{28}$. $Ca_{15}Si_{20}O_{10}N_{30}:Eu^{2+}$ emits a strong red light at UV to blue-light excitations. Moreover, the energy transfer among activators located at 5 different crystallographic sites was also studied. What' more, his group studied the energy transfer between Eu^{2+} ions at two different crystallographic site in Sr_2SiO_4,[22] $Sr_2Si_5N_8$[23] and $La_{4-x}Ca_xSi_{12}O_{3+x}N_{18-x}$.[24] The energy transfer among Eu^{2+} activators residing at different local environments in $CaAlSiN_3$ was also studied.[25] However, there are few literatures studying the energy transfer of Ce^{3+} located at different crystallographic

sites. Here we report $Ca_{15}Si_{20}O_{10}N_{30}:Ce^{3+}$ for near-UV LEDs which emits blue to green light as the content of Ce^{3+} increases. Besides, the decay behavior was studied in detail to interpret the energy transfer between various Ce^{3+} activators located at different coordination environments. In addition, the thermal quenching property was also studied.

2. Experimental section

Samples of $Ca_{15(1-x)}Si_{20}O_{10}N_{30}:xCe^{3+}$ ($0.01 \leq x \leq 0.05$) investigated in this work were synthesized through solid state reactions. CaO (A. R.), Si_3N_4 (Sigma-Aldrich 99.9%), CeO_2 (99.99%) were employed as raw materials. Moreover, 4 wt% graphite was added to reduce the oxygen in the reaction environment. These raw materials in the desired ratio were mixed in an agate mortar by adding an amount of ethanol and then grinded for 30 min. Finally, the mixture was placed into BN crucibles and then fired at 1450 ℃ under NH_3/N_2 atmosphere for 4 h in an electric furnace. After firing, the samples were cooled to room temperature in the furnace and ground again into powder for subsequent use.

All measurements were made on finely ground powder. The phase purity of samples was analyzed by X-ray diffraction (XRD) using a D2 PHASER X-ray Diffractometer with Ni-filtered Cu Kα radiation. Structure refinement was performed using the Rietveld method,[26] using the program GSAS.[27] Photoluminescence (PL) and PL excitation (PLE) spectra were measured at room temperature using a FLS-920T fluorescence spectrophotometer equipped with a 450 W Xe light source and double excitation monochromators. The PL decay curves were measured by a FLS-920T fluorescence spectrophotometer with a nF900 nanosecond flashlamp as the light source. High temperature luminescence intensity measurements were carried out by using an aluminium plaque with cartridge heaters; the temperature was measured by thermocouples inside the plaque and controlled by using a standard TAP-02 high temperature fluorescence controller. The powder morphology was observed by a field emission scanning electron microscope (FESEM; S-4800, Hitachi, Japan), transmission electron microscopy (TEM) and high-resolution transmission electron microscopy (HRTEM, FEI Tecnai F30, operated at 300 kV). The elemental compositions were examined with the FESEM equipped with an Energy Dispersive spectrometer (EDS) system.

3. Results and discussion

Phase identification and crystal structure

Fig. 1(a) shows the experimental (crosses), calculated (solid line), and difference (bottom) results of the XRD profiles for the Rietveld refinement of $Ca_{15}Si_{20}O_{10}N_{30}$ host. $Ca_{15}Si_{20}O_{10}N_{30}$ crystallizes in a cubic unit cell with space group $Pa\bar{3}$. For $Ca_{15}Si_{20}O_{10}N_{30}$ crystal, the lattice parameters were determined to be a = b = c = 15.4195 (3) Å and the refinement finally converged to R_{wp} = 9.88% and R_p = 7.35%. The XRD patterns of Ce^{3+} doped phosphors with different doping contents are illustrated in Fig. 1(b), which match well with the calculated XRD patterns, indicating that the obtained samples are all of single phase.

The simulation of the crystal structure of $Ca_{15}Si_{20}O_{10}N_{30}$ using Rietveld refinement is shown in Fig. 2. The $Ca_{15}Si_{20}O_{10}N_{30}$ structure provides 5 sites for Ca^{2+} ions; Ca1 are seven-coordinated with 5 N and 2 N/O atoms, Ca2 are six-coordinated with 4 N and 2 N/O atoms, Ca3 and Ca4 are eight-coordinated with 2 N and 6 N/O atoms, and Ca5 are six-coordinated with N atoms. It is noteworthy that Ca5, the 8c site with site symmetry of 3, is only 50% occupied in order to constitute the exact stoichiometry. The anion site consisted of 6 general sites and 2 special sites. Oxygen occupied 2 general sites according to the Ottinger's refinement result.[28] Accordingly, N1 (O1) and N2 (O2) sites were shared by oxygen (83.3%) and nitrogen (16.7%) in the case of $Ca_{15}Si_{20}O_{10}N_{30}$, while all the other anion sites were occupied by nitrogen only. Considering the radii of Ce^{3+} (1.03 Å) and Ca^{2+} (0.99 Å),[29] the Ce^{3+} activator could occupy the Ca sites in the $Ca_{15}Si_{20}O_{10}N_{30}:Ce^{3+}$ structure.

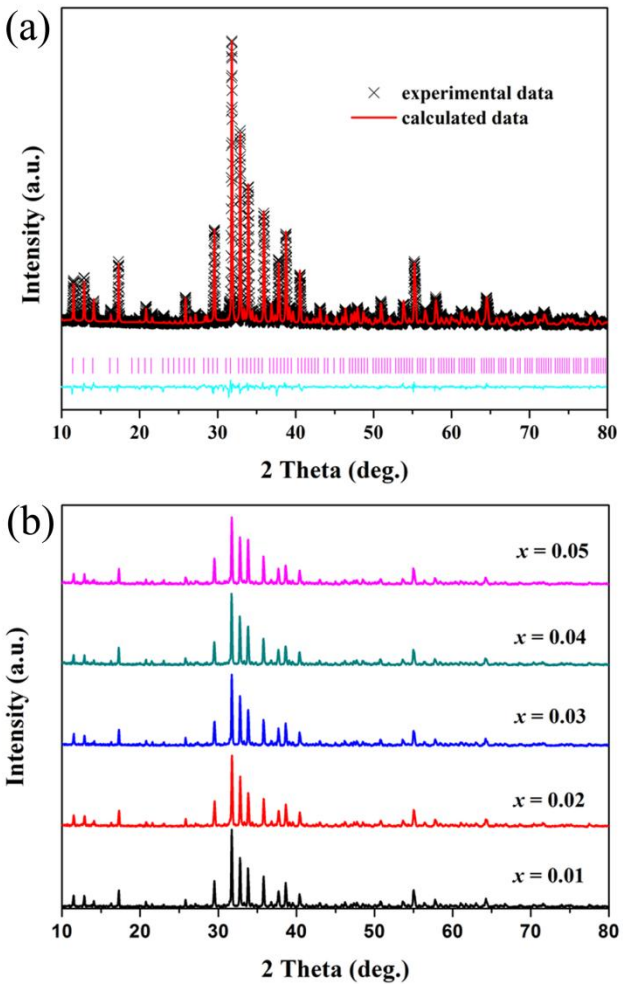

Fig. 1 (a) Experimental (crosses) and calculated (red solid line) XRD patterns of the $Ca_{15}Si_{20}O_{10}N_{30}$ host. The blue solid lines represent the difference between experimental and calculated data and the pink sticks mark the Bragg reflection positions. (b) XRD patterns of $Ca_{15(1-x)}Si_{20}O_{10}N_{30}:xCe^{3+}$ ($0.01 \leq x \leq 0.05$) samples.

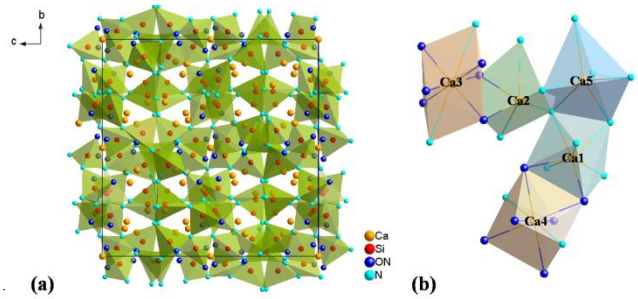

Fig. 2 (a) Crystal structure of the $Ca_{15}Si_{20}O_{10}N_{30}$ host viewed along [100] and (b) the coordination environments of the 5 Ca sites.

Fig. 3 (a-b) shows the SEM images of $Ca_{15}Si_{20}O_{10}N_{30}:Ce^{3+}$. The grains exhibit polyhedron shape and lamellar morphology with obvious agglomeration, which is also in accordance with the low-magnification as shown in Fig. 3(c). And the inset shows the HRTEM image. The inter-planar spacing was measured to be 3.14 Å, which matches well with the (224) inter planar distances of the cubic $Ca_{15}Si_{20}O_{10}N_{30}$. Fig. 4(d) shows the EDS spectrum, which indicates that the product has a chemical composition of Ca, Si, O and N, and the C peak may be ascribed to the residual graphite in the raw materials. These results also suggest that well-crystallized $Ca_{15}Si_{20}O_{10}N_{30}:Ce^{3+}$ powders have been obtained.

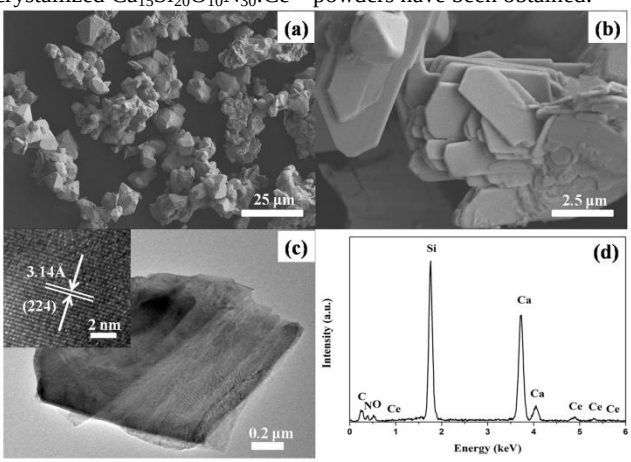

Fig. 3 (a-b) SEM, (c) TEM images (the inset shows the HRTEM image), and (d) EDS of $Ca_{15}Si_{20}O_{10}N_{30}:Ce^{3+}$.

Photoluminescence properties (the effect of Ce^{3+} activator content on the PL and decay behaviors)

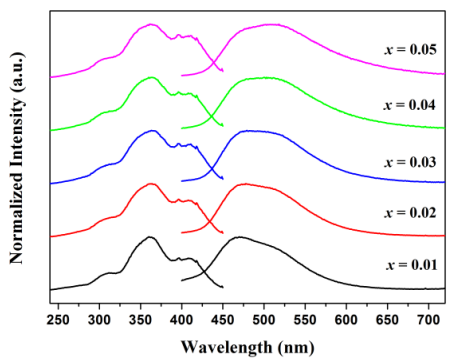

Fig. 4 Excitation and emission spectra (λ_{ex} = 365 nm) of $Ca_{15(1-x)}Si_{20}O_{10}N_{30}:xCe^{3+}$ ($0.01 \leq x \leq 0.05$) samples.

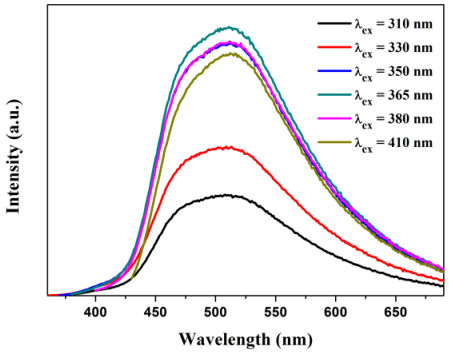

Fig. 5 Emission spectra of $Ca_{15}Si_{20}O_{10}N_{30}:0.05Ce^{3+}$ under different excitation wavelengths.

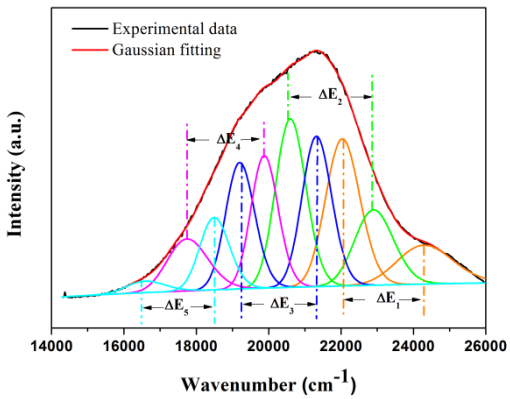

Fig. 6 Gaussian fitting of the emission band of $Ca_{15}Si_{20}O_{10}N_{30}:0.01Ce^{3+}$.

Fig. 4 shows the excitation and emission spectra for various Ce^{3+} activator contents. The peaks of the excitation bands of the samples doped with varying Ce^{3+} contents locate at about 310 nm, 365 nm and 410 nm, corresponding to the transition of Ce^{3+} from the $^2F_{5/2}$ ground state to the lowest 5d splitting level, making target samples interesting for application in near-UV white LEDs. Broad and asymmetric bands, peaking at about 470 nm and 520 nm, were observed in the emission spectra, which were originated from the 5d-4f transition of Ce^{3+}.

The $4f^1$-5d transition of Ce^{3+}, which includes the centre of gravity and its crystal-field splitting, is greatly influenced by the surrounding local structure.[30-32] Thus, the emission wavelengths of Ce^{3+} originating from Ca1 to Ca5 will be different. As depicted in Fig. 5, with the increase of the excitation wavelengths, the relative intensity ratio of 520 nm to 470 nm increases, showing that the emission corresponds to the transition from the 5d excited state to the $4f^1$ ground state of more than one Ce^{3+} ion.

It is accepted that the emission of Ce^{3+} can be attributed to the transitions from the lowest 5d excited state to the $^2F_{5/2}$ and $^2F_{7/2}$ ground states, which results in the fact that two distinguished emission spectra with a theoretical energy value of about 2000 cm^{-1} can be decomposed.[33] Accordingly, the emission band of $Ca_{15}Si_{20}O_{10}N_{30}:0.01Ce^{3+}$ was decomposed into ten well-separated Gaussian components (in Fig. 6) with maximum wavenumbers at 24272 and 22026 cm^{-1}, 22883 and 20618 cm^{-1}, 21322 and 19231 cm^{-1}, 19881 and 17762 cm^{-1}, 18518 and 16584 cm^{-1}, respectively. The above values are divided into five groups with ΔE_1 = 2246 cm^{-1}, ΔE_2 = 2265 cm^{-1}, ΔE_3 = 2091 cm^{-1}, ΔE_4 = 2119 cm^{-1} and

ΔE_5 = 1934 cm^{-1}, respectively. This further verifies that Ce^{3+} will occupy five different Ca^{2+} sites in the present $Ca_{15}Si_{20}O_{10}N_{30}$ host.

According to the refined structural data, the Ca3 and Ca4 polyhedrons consisted of 6 N/O ligands and 2 N ligands. This means that the local environment around the Ce^{3+} activator located at the Ca3 and Ca4 sites is composed mostly of oxygen, so that a blue shift could be anticipated. Thus, it is deduced that the highest-energy (24272 and 22026 cm^{-1}, 22883 and 20618 cm^{-1}) peaks are assigned to the transitions of Ce^{3+} occupying the Ca3 or Ca 4 site. However, Ca3 and Ca4 could not be distinguished clearly because the bond length data are reversed. The Ca3 site has a shorter distance to the O-N shared ligand and a longer distance to the pure nitrogen ligand, and *vice versa* for the Ca4 site. Furthermore, there was no oxygen in the Ca5 polyhedron, which will lead to the lowest-energy emission peaks (18518 and 16584 cm^{-1}). Nevertheless, the intermediate Gaussian peaks were not assigned due to the complexity. Namely, Ca1 site was composed of more N ligands while Ca2 site has a shorter average bond length.

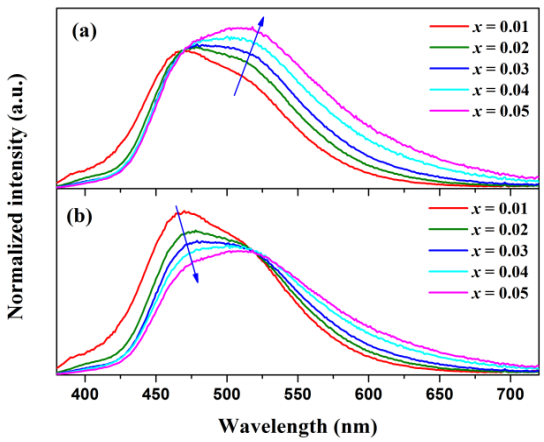

Fig. 7 Normalized PL spectra for $Ca_{15(1-x)}Si_{20}O_{10}N_{30}$:$xCe^{3+}$ ($0.01 \le x \le 0.05$) samples. (a) The blue emission intensities of Ce^{3+} at 470 nm are set as the standard. (b) The green emission intensities of Ce^{3+} at 520 nm are set as the standard.

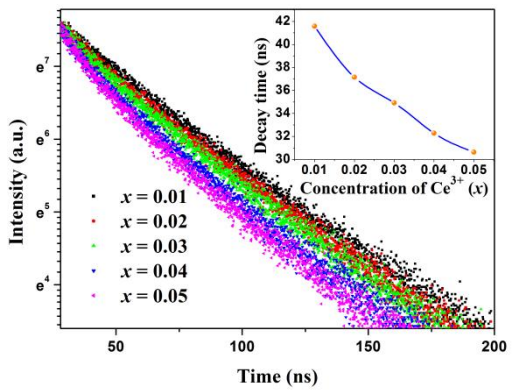

Fig. 8 The decay curves detected at 470 nm for various Ce^{3+} contents. The inset shows the variation of τ with increasing Ce^{3+} contents.

Fig. 7 shows normalized PL spectra for $Ca_{15(1-x)}Si_{20}O_{10}N_{30}$:$xCe^{3+}$ ($0.01 \le x \le 0.05$) samples. It is found that the PL spectra shift to longer wavelengths with the increase of Ce^{3+} content. At the same time, the dominated wavelength of the PL spectra changes from about 470 nm to 520 nm as the Ce^{3+} content increases. To explain this phenomenon, two possible reasons are proposed as follows. Firstly, with increasing the Ce^{3+} content, the reabsorption begins to reduce the high-energy wing of Ce^{3+} emission band, which also causes the redshift of the emission band.[34] Secondly, the energy transfer between Ce^{3+} ions with different coordination environments play an important role in the redshift, which will be further discussed below.

The decay curves for various Ce^{3+} contents at an excitation of 365 nm and monitored at 470 nm were measured (see Fig. 8). A typical concentration-quenching behaviour is observed, which shows that a higher Ce^{3+} content gives rise to a faster decay. The decay curves were found following the equation as follows:[35]

$$I(t) = A_1 \exp(-t/\tau_1) + A_2 \exp(-t/\tau_2) \quad (1)$$

where $I(t)$ is the luminous intensity at time t. τ_1 and τ_2 are short- and long-decay components and A_1 and A_2 are the constants, respectively. On the basis of equation 1, the luminescence lifetimes of Ce^{3+} monitored at 470 nm are determined to be 41.59, 37.15, 34.92, 32.29 and 30.63 ns for Ce^{3+} contents of 0.01, 0.02, 0.03, 0.04 and 0.05, respectively. As expected, the PL decays faster and the decay curve becomes more curved as the Ce^{3+} content increases, which is a strong evidence of brisk energy transfer, and eventually leads to concentration quenching.

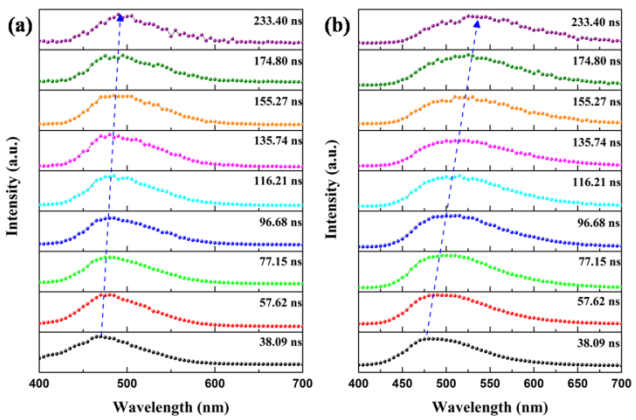

Fig. 9 TRES of (a) $Ca_{15}Si_{20}O_{10}N_{30}$:$0.01Ce^{3+}$ and (b) $Ca_{15}Si_{20}O_{10}N_{30}$:$0.02Ce^{3+}$.

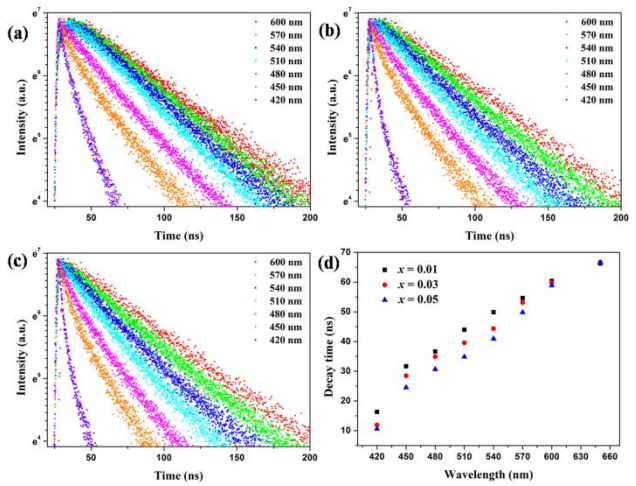

Fig. 10 Decay curves detected at various emission wavelengths for

$Ca_{15(1-x)}Si_{20}O_{10}N_{30}$:$xCe^{3+}$ (a) x = 0.01, (b) x = 0.03, (c) x = 0.05, and (d) calculated decay times.

To further realize the energy transfer between the donor and the acceptor, the time-resolved emission spectra (TRES) of $Ca_{15(1-x)}Si_{20}O_{10}N_{30}$:$xCe^{3+}$ (x = 0.01 and 0.02) were measured. We defined the donor as the Ce^{3+} located at a certain Ca site that exhibited the higher-energy emission, and the acceptor as the Ce^{3+} located at a certain Ca site that exhibited the lower-energy emission.

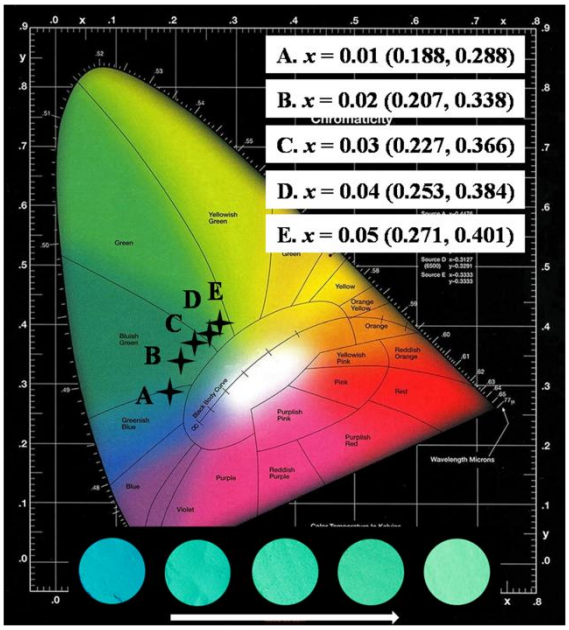

Fig. 11 CIE chromaticity diagram for $Ca_{15}Si_{20}O_{10}N_{30}$:$xCe^{3+}$ ($0.01 \leq x \leq 0.05$) phosphors and the sample photos (the bottom) under 365 nm excitation.

The TRES of $Ca_{15}Si_{20}O_{10}N_{30}$:$0.01Ce^{3+}$ and $Ca_{15}Si_{20}O_{10}N_{30}$:$0.02Ce^{3+}$ are depicted in Fig. 9. We didn't give the deconvoluted spectra in the initial stage of the time evolution for them because it is difficult to deconvolute the spectra to 10 Gaussian components. From Fig. 9(a) we can find that as the time delays, the shape of the spectra has little change but for a little redshift. The little redshift manifests that there is still a little energy transfer exists because the content of 1% Ce activator is not dilute enough to guarantee little chance of interaction with the quenching site and no chance for interactivator energy transfer. On the other hand, as the time delays, the TRES of $Ca_{15}Si_{20}O_{10}N_{30}$:$0.02Ce^{3+}$ exhibits an obvious change in the shape and a large redshift in the peak position, which is due to the fact that as the Ce^{3+} content increases, the acceptor components in the lower energy side (longer wavelength side) get stronger while the donor components in the higher energy side are weakened. By comparing the TRES of $Ca_{15}Si_{20}O_{10}N_{30}$:$0.01Ce^{3+}$ and $Ca_{15}Si_{20}O_{10}N_{30}$:$0.02Ce^{3+}$, we can conclude that the energy transfer rate is enhanced when the interactivator distance is reduced at a higher Ce^{3+} content, which leads to the annihilation of the high-energy side (donor side) emission and simultaneously activated the low-energy side (acceptor side) emission. Therefore, the higher-energy side emission was quenched and eventually led to the redshift. This process sufficiently explains the origin for the redshift caused by the increased Ce^{3+} content.

The decay curves detected at various emission wavelengths for $Ca_{15}Si_{20}O_{10}N_{30}$:$xCe^{3+}$ x = 0.01, 0.03 and 0.05 are depicted in Fig. 10(a-c). The decay curve varies as a function of the emission wavelength, namely, the higher-energy side (shorter wavelength) decays much faster than the lower-energy side (longer wavelength) for all Ce^{3+} contents. Moreover, the decay-time difference for the decay curves detected at 420 nm (higher-energy side) and 600 nm (lower-energy side) becomes more considerable when the Ce^{3+} content increases. This finding led to the conclusion that active energy transfer took place between Ce^{3+} activators, each of which has a distinct site environment. This sort of the energy transfer seems associated with the redshift. Another evidence for the energy transfer is the decay curve shape as shown in Fig. 10. The decay gradually gets less linear as the detection wavelength decreases to the donor side. This is a typical decay behaviour of the donors with a higher acceptor density in the vicinity.[36] The 5 different crystallographic Ca sites are not the direct reason for the varying decay time as a function of the detection wavelength, but the energy transfer between various Ce^{3+} activators located at different coordination environments, should be the direct reason,[21] and hence, the redshift.

The x and y values of the CIE chromaticity coordinates for the $Ca_{15}Si_{20}O_{10}N_{30}$:$xCe^{3+}$ phosphors are calculated and presented in Fig. 11, which were determined from the corresponding PL spectra at the excitation of 365 nm. By simply varying the content of Ce^{3+} from 0.01 to 0.05, tunable colors can be easily obtained under the NUV irradiation. The related tunable colors are visibly demonstrated by the digital photographs of the doped samples exposed to a 365 nm lamp. These results suggest it is possible to control the emission color by Ce^{3+} content.

Thermal quenching properties

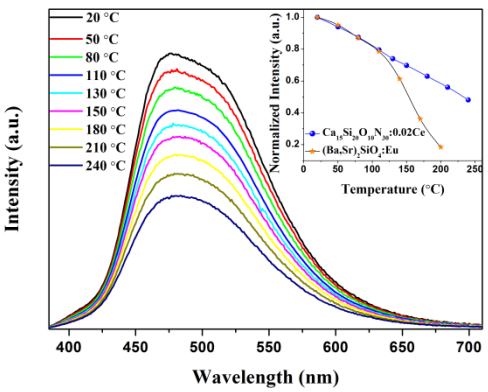

Fig. 12 Temperature dependence of PL spectra for $Ca_{15}Si_{20}O_{10}N_{30}$:$0.02Ce^{3+}$ under excitation at 365 nm. The integrated intensity versus temperature was depicted in the inset.

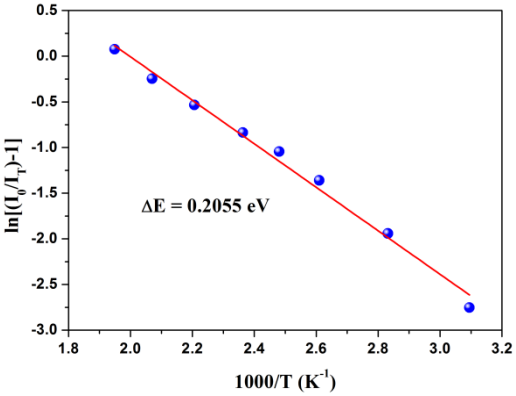

Fig. 13 Activation energy of $Ca_{15}Si_{20}O_{10}N_{30}$:0.02$Ce^{3+}$ phosphor.

The thermal stability of a phosphor is one of the important technological parameters for phosphors used in solid-state lighting, especially in high power WLEDs because it exerts considerable influence on the light output. To evaluate the influence of temperature on the luminescence, temperature dependence of the PL spectra for $Ca_{15}Si_{20}O_{10}N_{30}$:0.02$Ce^{3+}$ under excitation at 365 nm is shown in Fig. 12. The relative emission intensity of the $Ca_{15}Si_{20}O_{10}N_{30}$:0.02$Ce^{3+}$ phosphor decreases marginally as the temperature increases. The observation can be rationalized by the fact that increasing temperature has increased the population of higher vibration levels, the density of phonons and the probability of non-radiative transfer (energy migration defects). The emission spectrum of the phosphor has little shift as the temperature increases, which is indicative of the high stability of its chromaticity to temperature. The inset of Fig. 12 displays and compares the temperature dependence of PL intensity of $Ca_{15}Si_{20}O_{10}N_{30}$:0.02$Ce^{3+}$ and the commercial phosphor (Ba, Sr)$_2SiO_4$:Eu^{2+}. It can be observed that the thermal stability of $Ca_{15}Si_{20}O_{10}N_{30}$:0.02$Ce^{3+}$ is nearly the same as that of (Ba, Sr)$_2SiO_4$:Eu^{2+} below 100 ℃. However, above 100 ℃, it is obvious that the thermal stability of $Ca_{15}Si_{20}O_{10}N_{30}$:0.02$Ce^{3+}$ is superior to that of (Ba, Sr)$_2SiO_4$:Eu^{2+}. Moreover, the quenching temperature T_{50}, which is defined as the temperature at which the emission intensity is 50% of its original value, is 153 ℃ and 233 ℃ for (Ba, Sr)$_2SiO_4$:Eu^{2+} and $Ca_{15}Si_{20}O_{10}N_{30}$:0.02$Ce^{3+}$. For application in high power LEDs, the thermal stability of $Ca_{15}Si_{20}O_{10}N_{30}$:$Ce^{3+}$ needs to be further enhanced.

In order to understand the temperature dependence of emission intensity and to determine the activation energy for thermal quenching, the Arrhenius equation (equation 2) was fitted to the thermal quenching data of the $Ca_{15}Si_{20}O_{10}N_{30}$:0.02$Ce^{3+}$ phosphor.[37]

$$I_T = \frac{I_0}{1+c\exp\left(-\frac{\Delta E}{kT}\right)} \quad (2)$$

In equation (2), I_0 is the initial emission intensity; I_T is the intensity at different temperatures; ΔE is activation energy of thermal quenching; *c* is a constant for a certain host, and *k* is the Boltzmann constant (8.629×10^{-5} eV). Fig. 13 plots the relationship of ln[(I_0-I_T)-1] *vs.* 1000/T for the present $Ca_{15}Si_{20}O_{10}N_{30}$:0.02$Ce^{3+}$ phosphor, which is linear with a slope of -2.3819. According to equation (2), the activation energy ΔE of the phosphor was calculated to be 0.2055 eV. The relatively high activation energy further indicates that the $Ca_{15}Si_{20}O_{10}N_{30}$:0.02$Ce^{3+}$ has a good thermal stability.

4. Conclusions

In summary, a near-UV excited phosphor $Ca_{15}Si_{20}O_{10}N_{30}$:$Ce^{3+}$ was synthesized and studied. $Ca_{15}Si_{20}O_{10}N_{30}$ crystallizes in a cubic unit cell with space group $Pa\bar{3}$ and the lattice parameters were determined to be a = b = c = 15.4195 (3) Å. The color of the phosphor can be easily tuned from blue to green as the content of Ce^{3+} increases due to the energy transfer between various Ce^{3+} activators located at different coordination environments, which was verified by the TRES and the variation in decay rate with respect to the detection wavelength. Moreover, $Ca_{15}Si_{20}O_{10}N_{30}$:$Ce^{3+}$ exhibited a relatively low thermal quenching, and the T_{50} is measured to be 233 ℃. On the basis of the above experimental results, it is believed that the developed $Ca_{15}Si_{20}O_{10}N_{30}$:$Ce^{3+}$ is a potential color tunable component for near-UV excited white LEDs.

Acknowledgements

This work was supported by the National Natural Science Funds of China (Grant no. 51372105) and Specialized Research Fund for the Doctoral Program of Higher Education (no. 20120211130003). Thanks for the support of the Ministry of Industry and Information Technology of the Gansu Province.

Notes and references

**Key Laboratory for Special Function Materials and Structural Design of the Ministry of Education, School of Physical Science and Technology, Lanzhou University, Lanzhou,730000, China. E-mail: wyh@lzu.edu.cn; Fax: +86-931-8913554; Tel: +86-931-8912772*

1. S. Nakamura, T. Mukai and M. Senoh, *Appl. Phys. Lett.*, 1994, **64**, 1687-1689.
2. Y. Chiu, C. Huang, T. Lee, W. Liu, Y. Yeh, S. Jang, and R. Liu, *Opt. Express*, 2011, **19**, A331-A339.
3. T. Wang, X. Xu, D. Zhou, J. Qiu and X. Yu, *Mater. Res. Bull.*, 2014, 60, 876-881.
4. S. Nakamura, S. Pearton and G. Fasol, The blue laser diode: the complete story, Springer-Verlag, Berlin, 2000, pp. 230-235.
5. J. McKittrick, M. Hannah, A. Piquette, J. Han, J. Choi, M. Anc, M. Galvez, H. Lugauer, J. Talbot and K. Mishra, *ECS J. Solid State Sci. Technol.*, 2013, **2**, R3119-R3131.
6. J. Zhou, Z. Xia, M. Yang and K. Shen, *J. Mater. Chem.*, 2012, **22**, 21935.
7. N. Komuro, M. Mikami, Y. Shimomura, E. G. Bithell and A. K. Cheetham, *J. Mater. Chem. C*, 2015, **3**, 204-210.
8. A. Setlur and U. Happek, *J. Solid State Chem.*, 2010, **183**, 1127-1132.
9. R.-J. Xie, Y. Q. Li, N. Hirosaki and H. Yamamoto, *Nitride Phosphors and Solid-State Lighting*, CRC Press, New York, 2011.
10. J. H. Ryu, H. S. Won, Y.-G. Park, S. H. Kim, W. Y. Song, H. Suzuki, C.-B. Yoon, D. H. Kim, W. J. Park and C. Yoon, *Electrochem. Solid-State Lett.*, 2010, **13**, H30-H32.
11. L. Fachun, B. Lijing, Y. Zhiping and L. Quanlin, *J. Rare Earths*, 2012, **30**, 851-855.
12. Y. Ma, F. Xiao, S. Ye and Q. Zhang, *J. Electrochem. Soc.*, 2012, **159**, H358-H362.
13. W. Y. Huang, F. Yoshimura, K. Ueda, Y. Shimomura, H. S. Sheu, T. S. Chan, H. F. Greer, W. Zhou, S. F. Hu, R. S. Liu and J. P. Attfield, *Angew. Chem. Int. Ed. Engl.*, 2013, **52**, 8102-8106.
14. Y. Q. Li, G. de With and H. Hintzen, *J. Alloys Compd.*, 2004, **385**, 1-11.
15. X.-M. Wang, X. Zhang, S. Ye and X.-P. Jing, *Dalton Trans.*, 2013, **42**, 5167-5173.

16. T. Suehiro, N. Hirosaki, R.-J. Xie and T. Sato, *Appl. Phys. Lett.*, 2009, **95**, 051903.
17. B. Dierre, R.-J. Xie, N. Hirosaki and T. Sekiguchi, *J. Mater. Res.*, 2007, **22**, 1933-1941.
18. C. H. Hsu, B. M. Cheng and C. H. Lu, *J. Am. Ceram. Soc.*, 2011, **94**, 2878-2883.
19. D. Deng, S. Xu, X. Su, Q. Wang, Y. Li, G. Li, Y. Hua, L. Huang, S. Zhao and H. Wang, *Mater. Lett.*, 2011, **65**, 1176-1178.
20. W. B. Park, S. P. Singh, C. Yoon and K.-S. Sohn, *J. Mater. Chem. C*, 2013, **1**, 1832-1839.
21. W. B. Park, S. P. Singh, C. Yoon and K.-S. Sohn, *J. Mater. Chem.*, 2012, **22**, 14068.
22. D. Ahn, N. Shin, K. D. Park and K.-S. Sohn, *J. Electrochem. Soc.*, 2009, **156**, J242-J248.
23. K.-S. Sohn, S. Lee, R.-J. Xie and N. Hirosaki, *Appl. Phys. Lett.*, 2009, **95**, 121903.
24. W. B. Park, Y. Song, M. Pyo and K.-S. Sohn, *Opt. Lett.*, 2013, 38, 1739-1741.
25. S. Lee and K.-S. Sohn, *Opt. Lett.*, 2010, **35**, 1004-1006.
26. H. Rietveld, *J. Appl. Crystallogr.*, 1969, **2**, 65-71.
27. A. C. Larson and R. B. Von Dreele, *General Structure Analysis System. LANSCE, MS-H805, Los Alamos, New Mexico*, 1994.
28. F. Ottinger, Ph. D. Thesis, Eidgenössischen Technischen Hochschule, Zürich, Diss. ETH Nr., 2004, p. 15624.
29. R. D. Shannon, *Acta Crystallogr.*, 1976, **32**, 751-767.
30. P. Dorenbos, *J. Phys.: Condens. Matter*, 2003, **15**, 4797-4807.
31. P. Dorenbos, *Phys. Rev. B*, 2000, **62**, 15650-15659.
32. B. Zhang, X. Yu, T. Wang, S. Cheng, J. Qiu and X. Xu, *J. Am. Ceram. Soc.*, 2015, **98**, 171-177.
33. Y. Li, Y. Shi, G. Zhu, Q. Wu, H. Li, X. Wang, Q. Wang and Y. Wang, *Inorg Chem*, 2014, 53, 7668-7675.
34. J. Zhong, W. Zhuang, X. Xing, R. Liu, Y. Li, Y. Liu and Y. Hu, *J. Phys. Chem. C*, 2015, **119**, 5562-5569.
35. F. Kang, Y. Zhang and M. Peng, *Inorg. Chem.*, 2015, **54**, 1462-1473.
36. B. Di Bartolo, in *Energy Transfer Processes in Condensed Matter*, B. Di Bartolo and A. Karipidou, eds. (Plenum, 1984), p. 103
37. W.-R. Liu, C.-W. Yeh, C.-H. Huang, C. C. Lin, Y.-C. Chiu, Y.-T. Yeh and R.-S. Liu, *J. Mater. Chem.*, 2011, **21**, 3740-3744.

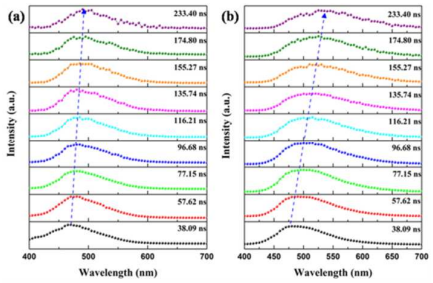

The dominant emission wavelength can be tuned from about 470 nm to 520 nm as the content of Ce^{3+} increases.